Surface & Coatings Technology 223 (2013) 87–91

Contents lists available at SciVerse ScienceDirect

Surface & Coatings Technology

journal homepage: www.elsevier.com/locate/surfcoat

Finite element analysis of crack propagation and fracture mechanical properties of freestanding 8 wt.% Y_2O_3–ZrO_2 coatings

X.S. Yang [a,b], J. Wan [a,b], C.Y. Dai [a,b], Y. Zhang [a,b], W.G. Mao [a,b,*], Y.C. Zhou [a,b], C. Lu [c]

[a] Key Laboratory of Low Dimensional Materials & Application Technology, Ministry of Education, Xiangtan University, Hunan 411105, China
[b] Faculty of Materials, Optoelectronics and Physics, Xiangtan University, Hunan 411105, China
[c] Department of Mechanical Engineering, Curtin University, Western Australia 6845, Australia

ARTICLE INFO

Article history:
Received 21 September 2012
Accepted in revised form 21 February 2013
Available online 1 March 2013

Keywords:
Thermal barrier coating
Fracture toughness
Finite element model
Energy release rate
Single edge notched beam

ABSTRACT

With the help of a digital image correlation technique, fracture strength and fracture toughness of freestanding 8 wt.% Y_2O_3–ZrO_2 (8YSZ) coatings were directly measured by single edge notched bending (SENB) tests. An extended finite element model (XFEM) was established to simulate the fracture process of notched 8YSZ samples. Its energy release rate was estimated by the known fracture strength and Young's modulus. Within the linear elastic brittle fracture, the calculated energy release rate was transformed into the corresponding fracture toughness, which is in good agreement with the experimental results by SENB. The obtained material properties of XFEM in this work would play a crucial role in predicting the reliability and durability of TBCs with irregular geometry in the future.

1. Introduction

Thermal barrier coatings (TBCs) have attracted an increasing attention in aircrafts and gas-turbines owing to their excellent wear resistance, corrosion resistance and thermal insulation. They can prolong the operation life of metal substrate and enhance the thermal efficiency of engines. A TBC system usually consists of ceramic coating (generally 8 wt.% Y_2O_3–ZrO_2 or 8YSZ), thermally grown oxide, bond coat and substrate [1]. However, the mechanical property evolution and premature adhesion failure of the ceramic coatings subjected to the mechanical loads, thermal/residual stresses, sintering and thermal shock in service have strongly affected their reliabilities and applications [2,3]. Recently, various experimental and simulation methods have been developed to evaluate the fracture strength and interface adhesion of different coating systems. In particular, the mechanical properties and fracture characteristics of 8YSZ coating have been widely studied by using tensile [4–8], indentation [9–13], compressions [14], shear [15] and bending tests [16–19]. Because most of TBC systems, frequently used in turbine blades and vans, have complex and irregular geometrical structures, it is inconvenient and difficult to use experimental methods and theoretical models to estimate their reliability and durability under severe environments. Thus, we have to resort to numerical analysis such as the finite element method (FEM), which has been used to the analysis of stress–strain fields, temperature distribution, cracking nucleation and propagation of TBC systems. The corresponding mechanical parameters such as critical energy release rate, stress intensity factor were evaluated [15,20,21]. For example, Sadowski et al. have discussed the damage and progressive fracturing process of the most dangerous cross-sections of a blade under real working conditions by an extended finite element method (XFEM) [22]. In judgment of the initiation and propagation of cracks in ceramic coatings during finite element simulations in previous works, the criterion is generally assumed that the maximum principal stress in coating exceeds its fracture strength. Furthermore, to validly predict the damage accumulation, cracking and fracture process of a TBC system by XFEM, several important material parameters such as Young's modulus E, fracture strength σ_b and critical energy release rate G_I must be determined with the aid of experiments. To the best of our knowledge, however, only a few attempts have been made in the earlier work to directly study these material parameters of XFEM of air plasma sprayed (APS) TBCs by precise experimental tests.

In this work, freestanding 8YSZ coating samples were prepared by APS technique and their mechanical properties including σ_b and fracture toughness K_{IC} before and after thermal cycling were determined by single edge notched beam (SENB) and digital image correlation (DIC) techniques. Using the measured E, σ_b and assumed G_I, various simulated loading–deflection curves corresponding to a given 8YSZ sample were obtained by commercial ABAQUS software. In comparison with the simulated and experimental curves, the most appropriate G_I value can be estimated and then it was transformed into the corresponding K_{IC} by linear elastic brittle fracture mechanics. It was found that K_{IC} deduced by XFEM were consistent well with that by SENB tests. For different types of freestanding 8YSZ coatings with thermal cycling, the corresponding material parameters of XFEM would be helpful in predicting the damage, cracking and spallation

* Corresponding author at: Faculty of Materials, Optoelectronics and Physics, Xiangtan University, Hunan 411105, China. Tel.: +86 731 58298580; fax: +86 731 58292468.
E-mail address: ssamao@126.com (W.G. Mao).

0257-8972/$ – see front matter © 2013 Elsevier B.V. All rights reserved.
http://dx.doi.org/10.1016/j.surfcoat.2013.02.034

of TBCs deposited on turbine blades under complex service conditions. Finally, the fracture morphologies of 8YSZ samples were observed by scanning electronic microscope (SEM) and the effect of heat treatment on mechanical properties was discussed in briefly.

2. Experimental details

2.1. Sample preparation

To prepare the stand-alone thick 8YSZ coating, the 8YSZ powder with grain sizes of 20–60 μm was directly sprayed on an aluminum substrate with a size of 160 × 25 × 10 mm^3 by a Metco-Triplex I plasma gun (Sulzer Metco, Winterthur, Switzerland). During the air plasma spraying, the substrates were cooled with compressed air resulting in deposition temperatures between 200 and 250 °C. After completing the spraying process and cooling to the room temperature in air, the coated aluminum substrate was carefully incised into small bars by a commercial cutting machine (IsoMet® 4000). The top 8YSZ coating for each bar was obtained after the aluminum substrate was etched with potassium hydroxide. And then these freestanding 8YSZ coatings were cut into many rectangular shape samples with 20 × 3 × 4 mm^3. To consider the sintering effect, most of them were subjected to heat treatments in a high temperature furnace. Each thermal cycling consists of 10 min heating to the desire surface temperature of 1273 K, and then holding at this temperature for 60 min followed by a 10 min forced-air-quenching. The type of thermal cycle includes 0, 50, 100, 150, 200 and 300 times. The number for each type sample is 7 and the total number of sample is 42. All samples were polished with 2.5 μm diamond paste. The SENB samples were fabricated and loaded according to the ASTM standard E1820-05a [23], where the notch was cut across the 3 mm face, perpendicular to the length of the bending bar. The narrow notch tip radii are about 5–10 μm by a commercial cutting machine with a thin diamond saw blade. The notch depths of ~1.5 mm were used, as shown in Fig. 1. The samples were handled by hydrochloric acid to reduce the influence of surface work hardening. They were also carefully cleaned by ultrasonic oscillator with distilled water and completely dried.

2.2. SENB tests

SENB tests were performed by a universal testing machine (No. WDTI-5) with the displacement rate control mode at a speed of 0.01 mm/min. The bending loads increase linearly up to the maximum load at which the notched 8YSZ samples break down. A DIC technique was used to real-time monitor the strain evolution near the notch tip region, as shown in red dashed region of Fig. 1. The strain data burst can accurately reflect the crack nucleation and propagation of the notched sample under bending, and then the corresponding load can be determined as the critical bending load [5]. Prior to the DIC test, patterns were prepared by spraying a thin layer of black and white paint with airbrush guns. A 1624 × 1236 pixels charge coupled device camera equipped with a lens of 50 mm focal length was used to *in-situ* measure the macroscopic morphology and strain evolution of the monitored region (4 × 3 mm^2) with a sampling rate of two images per second (see Fig. 1). The relevant post-processing was achieved with the commercially available DIC software (ARAMIS) to analyze the evolution of strain field data. The measuring error in strain is limited less than 0.05% by the specifications and settings [24]. All experimental data, including the critical bending load, strain field, crack initiation and propagation path, were *in-situ* recorded by computers, which were used to estimate other material properties of 8YSZ samples. For SENB tests, σ_b and K_{IC} can be obtained by the following formulae [25,26], respectively,

$$\sigma_b = \frac{3FL}{2B(W-a)^2} \tag{1}$$

$$K_{IC} = Y \times \frac{3FL}{2BW^2} \times \sqrt{a} \tag{2}$$

where F denotes the bending load. a is the length of the notch. B and W are, respectively, the width and highness of the sample. L is the span between the two lower supporting points. Y is a factor by a / W. In the case of $L / W = 4$, Y can be represented by the following exponential polynomial [27],

$$Y = 1.93 - 3.07 \times \frac{a}{W} + 14.53 \times \left(\frac{a}{W}\right)^2 - 25.11 \times \left(\frac{a}{W}\right)^3 + 25.8 \times \left(\frac{a}{W}\right)^4. \tag{3}$$

3. Extended finite element model (XFEM)

As we know, for the finite simulations of two-dimensional fracture problem of brittle APS coatings with much inter-lamellar pores and micro cracks [28], the effect of microstructure factor on the estimation of mechanical properties of ceramic has been considered by the object oriented finite element modeling [29,30]. But it is usually limited to a two-dimensional fracture problem of brittle APS coatings. For simplicity, the effects of microstructure features on the mechanical properties of 8YSZ samples were ignored during XFEM in this work. Fig. 2 shows a three-dimensional XFEM of bending fracture process of freestanding 8YSZ sample, which consists of 6840 8-node linear brick reduced integration elements (C3D8R). Further refining of the current mesh shows little improvement in calculation accuracy. The indenter of the universal testing machine is regarded as a rigid surface and its motion under bending loads is controlled by a reference point. The bending loads during FEM were applied by controlling the displacement of the reference point. In order to simulate the brittle fracture process, the maximum principal stress criterion was introduced and it can be represented as [31]

$$f = \frac{\langle \sigma_{max} \rangle}{\sigma^0_{max}} \tag{4}$$

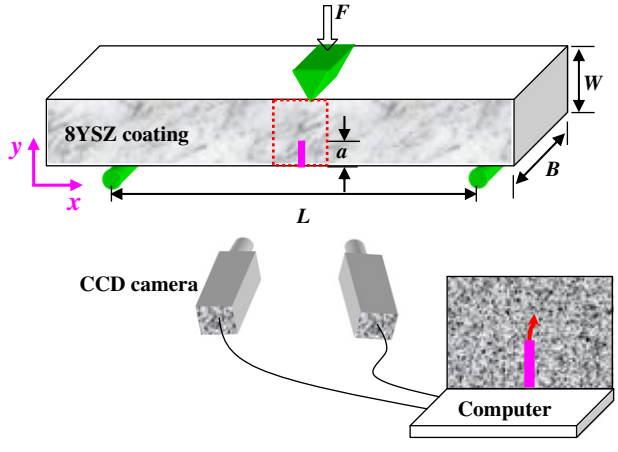

Fig. 1. Schematic of SENB test by the aid of DIC. The rectangle with dashed red line was defined as a region for DIC monitoring.

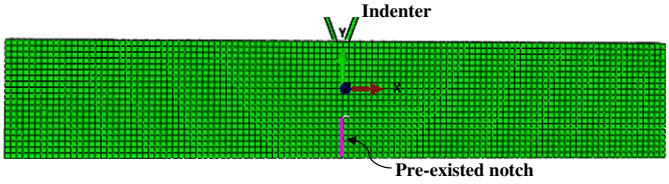

Fig. 2. Three-dimensional XFEM of a notched 8YSZ sample under SENB test.

where σ^0_{max} represents the allowable maximum principal stress of ceramic coatings, which is usually equal to σ_b. σ_{max} is the maximum principal stress under bending. Bracket < > in Eq. (4) indicates that a purely compressive stress state does not induce damage. Thus, damage is assumed to initiate once f reaches 1.0.

To reasonably set the material parameters of XFEM, E, σ_b and G_I must be given. In this work, E of all 8YSZ samples were determined by nanoindentation [32]. All indentations with Berkovich indenter were performed with the load control ($dP/dt = 30$ mN/s) at 300 K. The maximum load was set at 3 N and the dwelling time was 20 s. The 20 perfect indentations were carried out for each sample [32]. The σ_b of all 8YSZ samples were measured from the above SENB tests. The simulated load–deflection curves by XFEM were obtained by attempting different G_I values. Finally, an acceptable G_I value can be evaluated by comparing with the corresponding experimental curve in SENB test. The detailed XFEM procedure is shown in Fig. 3. According to the linear elastic brittle fracture, the corresponding K_{IC} can be deduced by G_I above [33]

$$K_{IC} = (EG_I)^{1/2}. \quad (5)$$

4. Results

4.1. Determination of σ_b and K_{IC} by SENB

A typical stain evolution near the pre-existed notch is shown in Fig. 4. As the bending load increases, DIC patterns reveal that the deformation on the cross-section becomes more heterogeneous (see inset (A)). When the test time t reaches 172 s, a strain concentration region appears around the notch tip in inset of Fig. 4, which slowly propagates along the y direction. As $t = 201$ s, the stain concentration region become more obvious and forms a small crack, as shown in inset (C) of Fig. 4. Furthermore, the crack starts to propagate parallel to the y axis at $t = 217$ s. The experimental data including the bending load, strain and time were recorded by a computer, which were used to evaluate σ_b and K_{IC}. For example, when the bending load tardily increases up to about 17.77 N, the DIC analysis shows that a crack begins to propagate. Therefore, the corresponding σ_b and K_{IC} can be obtained as 25.92 MPa and 1.66 MPa $m^{1/2}$ by Eqs. (1) and (2), respectively. The average σ_b and K_{IC} for samples before and after heat-treatments are listed in Table 1. The relevant K_{IC} changes from 1.12 MPa $m^{1/2}$ to 2.45 MPa $m^{1/2}$ prior to $N = 150$ thermal cycles, decreased to 1.62 MPa $m^{1/2}$ as $N = 300$.

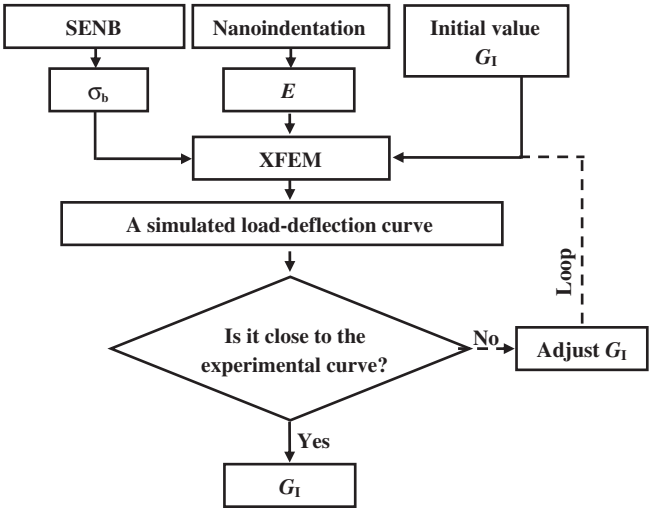

Fig. 3. The procedure of XFEM for estimating G_I.

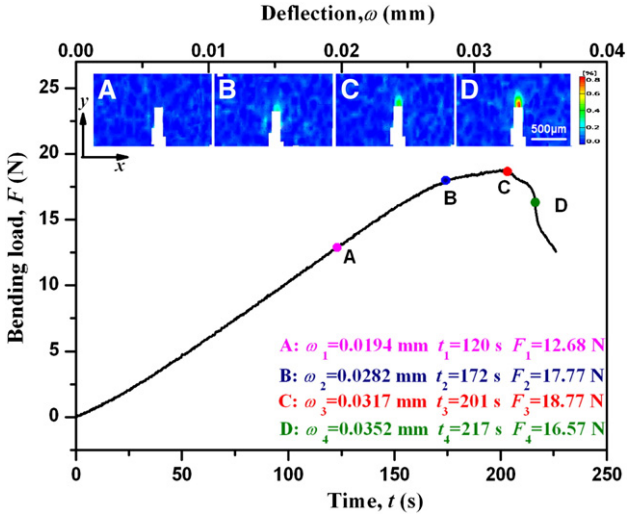

Fig. 4. A typical loading–deflection–time curve of 8YSZ under bending. A series of strain map insets shows the evolution of strains in the monitored area with the increase of bending loads.

4.2. Evaluation of G_I by XFEM

As shown in Fig. 5, many simulated load–deflection curves by assuming different G_I during XFEM match progressively with the true experimental curve, respectively. Here, the geometry size of the 8YSZ sample are $L = 18.5$ mm, $W = 4.5$ mm, $B = 1.4$ mm, and $a = 1.6$ mm, respectively. And $E = 32.4$ GPa, $\nu = 0.1$ and the average value of σ_b equals about 24.5 MPa. Comparing and analyzing the difference between the experimental and simulated load–deflection curves, G_I for freestanding 8YSZ coating after 300 thermal cycles can be evaluated as about 84 J/m^{-2} (see Fig. 5). Using the similar method, the G_I of other freestanding 8YSZ samples was evaluated and listed in Table 1.

4.3. SEM observations of fracture morphology

Fig. 6 displays several SEM images of typical fracture surface of as-sprayed and aged freestanding 8YSZ coatings after SENB tests. It can be seen that there are a large amount of pores in conjunction with splat structures for as-received sample, as shown in Fig. 6(a). It exhibits mainly inter-splat fracture mode. After 100 thermal cycles, a noticeable sintering phenomenon occurs owing to the phase transformation and substantial grain growth of 8YSZ ceramic [28] (see Fig. 6(b)). It may result in the increase of these mechanical properties, E, σ_b and K_{IC} of 8YSZ coating. The similar experimental phenomena have been reported in previous works [34–36]. As $N = 200$, partial regions show more noticeable sintering, densification and micro crack nucleation (see Fig. 6(c)). When N increases up to 300, more apparent macro-cracks and typical lamellar structure are observed, as displayed in Fig. 6(d). These micro cracks deduced from heat treatments would result in the decrease of the E, σ_b and K_{IC} of 8YSZ coating.

5. Discussion

5.1. Evolution of σ_b and K_{IC}

It is seen from Table 1 that σ_b by SENB tests increases from 35.66 ± 6.13 MPa at as-received to 71.76 ± 7.25 MPa at $N = 50$ with the increasing of thermal aging time. The main reason may result from high-temperature sintering, grain growth and phase transformation. Especially, the sintering process increases the fracture strength and decreases the fracture strain remarkably [37]. The

Table 1
Comparison of the experimental and numerical results of freestanding 8YSZ coatings.

N	E (GPa)	ε_{xx}^{cri}	σ_b[a] (MPa)	K_{IC}[b] (MPa $m^{1/2}$)	G_I[c] (J/m^{-2})	K_{IC}[d] (MPa $m^{1/2}$)
0	9.78 ± 1.00	0.28 ± 0.02	35.66 ± 6.13	1.12 ± 0.03	115	1.06
50	22.41 ± 1.20	0.23 ± 0.03	71.76 ± 7.25	1.73 ± 0.15	117	1.62
100	29.68 ± 2.23	0.19 ± 0.02	53.90 ± 1.87	2.00 ± 0.20	120	1.89
150	31.01 ± 1.34	0.18 ± 0.02	56.05 ± 0.72	2.45 ± 0.12	175	2.33
200	34.66 ± 1.57	0.15 ± 0.02	31.62 ± 1.21	1.71 ± 0.22	71	1.57
300	32.41 ± 2.68	0.17 ± 0.04	24.70 ± 0.40	1.62 ± 0.10	84	1.65

[a] σ_b was tested by SENB with Eq. (1).
[b] K_{IC} was directly deduced by SENB with Eq. (2).
[c] G_I was evaluated by XFEM with the known E and σ_b.
[d] K_{IC} was directly obtained by the simulated G_I and Eq. (5).

velocity of sintering activity is affected by the diffusion of the different atomic species determined in freestanding 8YSZ coating. In this work, the increase in fracture strength upon annealing occurs in a short period of time of about 50 h, which is similar to 20 h reported by Choi et al. [37]. In the earlier works, for freestanding 8YSZ samples, Ahmaniemi et al. have reporsted that σ_b by four-point bending changes from 39.70 ± 2.70 MPa at as-received to 91.30 ± 3.90 MPa after heat treatment 5 h at 1250 °C. Choi et al. have also found that σ_b starts from 37.0 ± 4.00 MPa and increases rapidly to about 80 MPa within 100 h, and then it keeps a steady state [37]. However, in this work, σ_b gradually decreases to 24.70 ± 0.40 MPa at $N = 300$. The reason may be due to the possible differences of spraying process parameters, heat treatment temperatures and experimental test methods. Although annealing can provide a sintering effect, it may also result in microcracks and micropore healing, grain growth, and densification [37]. Many tests show that most of mechanical properties for plasma-sprayed zirconia coatings increase significantly in 5–100 h, and then reach a plateau above 100 h or slightly decrease to some value.

It is found in Table 1 that the relationship of fracture toughness and annealing time follows the similar trend of the fracture strength in the as-sprayed as well as in the heat treated samples. In the previous studies, K_{IC} for as-received APS freestanding 8YSZ coatings is about 1.15 ± 0.07 MPa $m^{1/2}$ by asymmetric four-point bending tests at room temperature. On annealing, K_{IC} increased significantly within 100 h and reached a plateau value 2.60 ± 0.20 MPa $m^{1/2}$ [38]. Mao et al. have studied the evolution of microhardness, fracture toughness and residual stress of APS TBC system under thermal cycles by a modified Vickers indentation instrument coupled with three kinds of indentation models. They found that K_{IC} at the cross-section coating as a function of annealing time ranges from 0.7 to 1.2 MPa $m^{1/2}$ by Vickers indentation tests [9]. In this work, the initial value of K_{IC} is 1.12 ± 0.03 MPa $m^{1/2}$ and the maximum value is 2.45 ± 0.12 MPa $m^{1/2}$, as listed in Table 1. Thus, the results are in agreement with these available data.

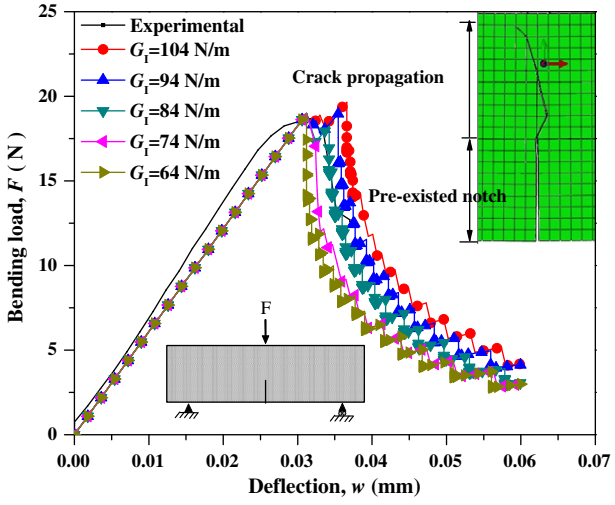

Fig. 5. The evaluation of critical energy release rate of 8YSZ sample by progressively comparing the experimental and simulated load–deflection curves, where $N = 300$. Inset shows the propagation of the pre-existed notch under bending.

5.2. Critical energy release rate

In Table 1, G_I for freestanding 8YSZ samples annealed with different aging times firstly increases from 115 J/m^{-2} at as-received to 175 J/m^{-2} as $N = 150$, but it gradually decreases to 84 J/m^{-2} when $N = 300$. The critical aging time is about 150 h. The evolution of G_I in our work is qualitatively in agreement with that obtained from four-point bending tests by Yamazaki et al. [39]. For as-received APS TBCs, $G_I = 115$ J/m^{-2} in this work is close to 140 J/m^{-2} [39] and slightly higher than the available experimental data, 50~70 J/m^{-2} [40–42]. The difference in measured strain energy release rate may be attributed to APS processing parameters, 8YSZ microstructure and test method. To compare with K_{IC} by SENB tests, the obtained G_I is, respectively, transformed into K_{IC} by Eq. (5) and also shown in Table 1. Because the E of 8YSZ coating changes with thermal cycle due to the sintering effect, the K_{IC} value by XFEM increases from the as-sprayed value of 1.06 MPa $m^{1/2}$ to 2.33 MPa $m^{1/2}$ as $N = 150$, and then decreases to 1.65 MPa $m^{1/2}$ when $N = 300$. Although test method and aging temperature have difference, our results are similar to that by four-point bending tests [39]. For as-received APS TBC coatings, the fracture toughness in our work is slightly higher than the range of 0.4–1.2 MPa $m^{1/2}$ in TBC systems [9,37,38,43]. It indicates that the evaluation of material properties of freestanding 8YSZ coating used in XFEM is credible, which are useful for predicting the failure behavior and lifetime of TBCs with irregular geometry.

6. Conclusions

The evolution and accurately measurements of mechanical parameters of freestanding 8YSZ coating play an important role in appraising the reliability and durability of TBCs. The freestanding 8YSZ samples were successfully prepared by APS technique. The corresponding mechanical properties were measured by SENB and DIC techniques. The bending failure process of 8YSZ was simulated by XFEM. Using the determined experimental data and attempting different energy release rate, the material parameters of XFEM were evaluated, which would be used to predict the delamination and spallation of TBC with irregular geometry. The main conclusions can be summarized as follows,

(1) The K_{IC} of freestanding 8YSZ coatings by SENB tests changes from 1.12 MPa $m^{1/2}$ to 2.45 MPa $m^{1/2}$ before $N = 150$, and then decreases to 1.62 MPa $m^{1/2}$ as $N = 300$. The corresponding σ_b firstly increases from 35.66 ± 6.13 MPa at as-received to 71.76 ± 7.25 MPa at $N = 50$ due to the sintering and

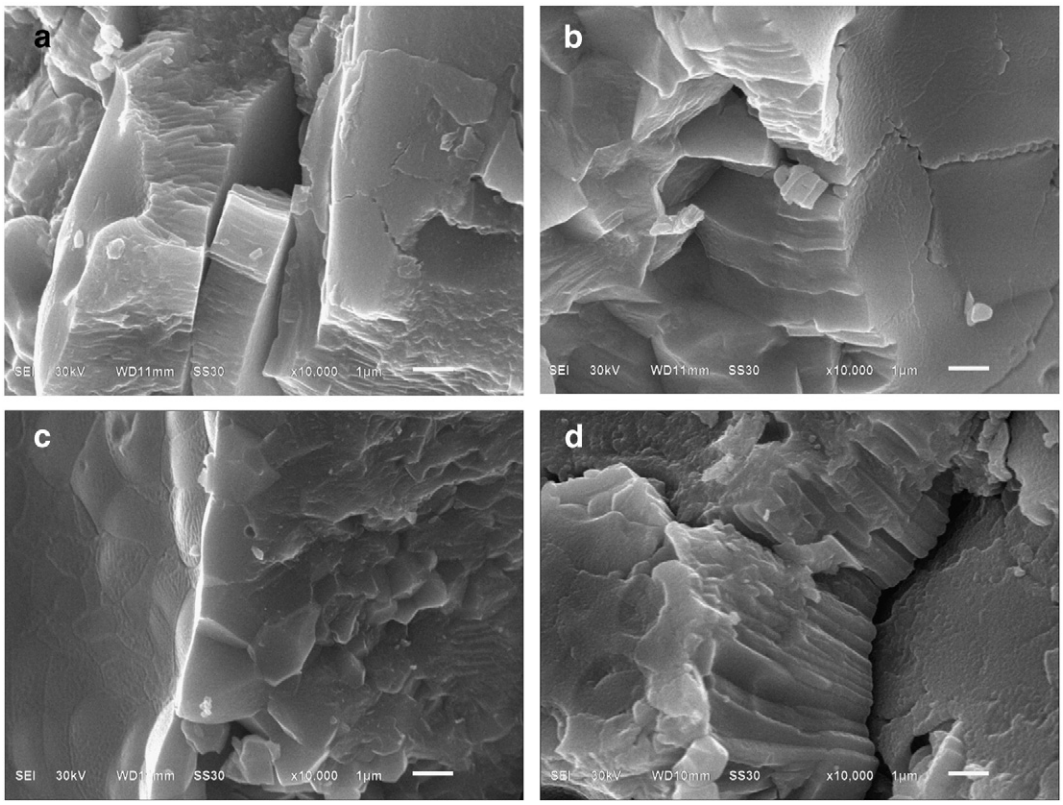

Fig. 6. Typical SEM micrographs of fracture surfaces of freestanding 8YSZ samples after SENB tests, (a) as-received, (b) heat-treated (100 cycles), (c) heat-treated (200 cycles), and (d) heat-treated (300 cycles).

densification, and then it slightly decreases to 24.70 ± 0.40 MPa when $N = 300$ because of the formation of much micro cracks.

(2) The G_I of 8YSZ coatings estimated by XFEM ranges from 71 to 175 J/m^{-2} for different heat-treated 8YSZ samples. The corresponding K_{IC} was deduced within the linear elastic fracture mechanics, which consists well with that by the SENB tests.

Acknowledgments

This work has been supported by the National Natural Science Foundations of China (no. 11102177, 11272276 and 51172192), the Natural Science Foundation of Hunan Province for Innovation Group (no. 09JJ7004), and the Program for Changjiang Scholars and Innovative Research Team in University (no. IRT1080).

References

[1] N.P. Padture, M. Gell, E.H. Jordan, Science 296 (2002) 280.
[2] A.G. Evans, M.Y. He, J.W. Hutchinson, Prog. Mater. Sci. 46 (2001) 249.
[3] X.Y. Xie, H.B. Guo, S.K. Gong, J. Therm. Spray Technol. 19 (2010) 1179.
[4] W.B. Yao, C.Y. Dai, W.G. Mao, C. Lu, L. Yang, Y.C. Zhou, Surf. Coat. Technol. 206 (2012) 3803.
[5] D.J. Wu, W.G. Mao, Y.C. Zhou, C. Lu, Appl. Surf. Sci. 257 (2011) 6040.
[6] W. Shen, F. Wang, Q. Fan, Z. Ma, X. Yang, Surf. Coat. Technol. 205 (2011) 2964.
[7] C.S. Ramachandran, V. Balasubramanian, P.V. Ananthapadmanabhan, Surf. Eng. 27 (2011) 217.
[8] Z.B. Chen, Z.G. Wang, S.J. Zhu, Surf. Coat. Technol. 205 (2011) 3931.
[9] W.G. Mao, J. Wan, C.Y. Dai, J. Ding, Y. Zhang, Y.C. Zhou, C. Lu, Surf. Coat. Technol. 206 (2012) 4455.
[10] T. Zisis, N.A. Fleck, Wear 268 (2010) 443.
[11] Y. Yamazaki, S. Kuga, T. Yoshida, Acta Metall. Sin. (Engl. Lett.) 24 (2011) 109.
[12] A. Dey, A.K. Mukhopadhyay, Int. J. Appl. Ceram. Tech. 8 (2011) 572.
[13] X. Wang, C. Wang, A. Atkinson, Acta Mater. 60 (2012) 6152.
[14] W.G. Mao, C.Y. Dai, Y.C. Zhou, Q.X. Liu, Surf. Coat. Technol. 201 (2007) 6217.
[15] Z. Xu, Y. Yang, P. Huang, X. Li, Acta Mater. 58 (2010) 5972.
[16] C. Pfeiffer, E. Affeldt, M. Göken, Surf. Coat. Technol. 205 (2011) 3245.
[17] P.F. Zhao, C.A. Sun, X.Y. Zhu, F.L. Shang, C.J. Li, Surf. Coat. Technol. 204 (2010) 4066.
[18] X. Wang, S. Tint, M. Chiu, A. Atkinson, Acta Mater. 60 (2012) 3247.
[19] J. Malzbender, R.W. Steinbrech, Surf. Coat. Technol. 209 (2012) 97.
[20] M. Bäker, Comput. Mater. Sci. 64 (2012) 79.
[21] H. Bhatnagar, S. Ghosh, M.E. Walter, Mech. Mater. 42 (2010) 96.
[22] T. Sadowski, P. Golewski, Comput. Mater. Sci. 64 (2012) 285.
[23] ASTM E1820-05a, Standard Test Method for Measurement of Fracture Toughness, ASTM International, West Conshohocken, PA 19428-2959, United States, 2005.
[24] W.G. Mao, D.J. Wu, W.B. Yao, M. Zhou, C. Lu, J. Appl. Phys. 110 (2011) 084903.
[25] J.B. Wachtman, Mechanical properties of ceramics, A Wiley-Interscience Publication, United States of America, 1996.
[26] X. Peng, N. Sridhar, D.R. Clarke, Mater. Sci. Eng. A 380 (2004) 208.
[27] W.F. Brown, J.E. Srawley, Plane Strain Crack Toughness Testing of High Strength Metallic Materials, American Society for Testing and Materials, Philadelphia, 1966.
[28] J. Wu, H.B. Guo, L. Zhou, L. Wang, S.K. Gong, J. Therm. Spray Technol. 19 (2010) 1186.
[29] Z. Wang, A. Kulkarni, S. Deshpande, T. Nakamura, H. Herman, Acta Mater. 51 (2003) 5319.
[30] N.P. Padture, A.D. Jadhav, E.H. Jordan, M. Gell, P. Miranzo, E.R. Fuller Jr., Acta Mater. 54 (2006) 3343.
[31] ABAQUS Version 6.10, Hibbit Karlsson and Sorensen, Inc., 2010. USA.
[32] Q. Chen, W.G. Mao, Y.C. Zhou, C. Lu, Appl. Surf. Sci. 256 (2010) 7311.
[33] B.R. Lawn, Fracture of Brittle Solids, Cambridge University Press, USA, 1993.
[34] S. Guo, Y. Kagawa, Scr. Mater. 50 (2004) 1401.
[35] J.A. Thompson, T.W. Clyne, Acta Mater. 49 (2001) 1565.
[36] F. Tang, J.M. Schoenung, Scr. Mater. 54 (2006) 1587.
[37] S.R. Choi, D. Zhu, R.A. Miller, J. Am. Ceram. Soc. 88 (2005) 2859.
[38] S.R. Choi, D. Zhu, R.A. Miller, Eng. Fract. Mech. 72 (2005) 2144.
[39] Y. Yamazaki, A. Schmidt, A. Scholz, Surf. Coat. Technol. 201 (2006) 744.
[40] S.Q. Guo, D.R. Mumm, A.M. Karlsson, Y. Kagawa, Scr. Mater. 53 (2005) 1043.
[41] Y. Zhao, A. Shinmi, X. Zhao, P.J. Withers, S. Van Boxel, N. Markocsan, P. Nylen, P. Xiao, Surf. Coat. Technol. 206 (2012) 4922.
[42] I. Hofinger, M. Oechsner, H.A. Bahr, M.V. Swain, Int. J. Fract. 92 (1998) 213.
[43] G. Thurn, G.A. Schneider, H.A. Bahr, F. Aldinger, Surf. Coat. Technol. 123 (2000) 147.